Обзор ArXiv:astro-ph, 25-29 марта 2019 года

От Сильченко О.К.

ArXiV: 1903.09202

400 pc imaging of a massive quasar host galaxy at a redshift of 6.6

BRAM P. VENEMANS,[1] MARCEL NEELEMAN,[1] FABIAN WALTER,[1,2,3] MLADEN NOVAK,[1] ROBERTO DECARLI,[4] JOSEPH F. HENNAWI,[5] AND HANS-WALTER RIX[1]

[1]*Max-Planck Institute for Astronomy, Königstuhl 17, D-69117 Heidelberg, Germany*
[2]*Astronomy Department, California Institute of Technology, MC105-24, Pasadena, CA 91125, USA*
[3]*National Radio Astronomy Observatory, Pete V. Domenici Array Science Center, P.O. Box 0, Socorro, NM 87801, USA*
[4]*Osservatorio di Astrofisica e Scienza dello Spazio di Bologna, via Gobetti 93/3, I-40129 Bologna, Italy*
[5]*Department of Physics, Broida Hall, University of California, Santa Barbara, California 93106-9530, USA.*

(Received 2019 February 2; Revised 2019 March 20; Accepted 2019 March 20)

ABSTRACT

We report high spatial resolution ($\sim 0\farcs076$, 410 pc) ALMA imaging of the dust continuum and the ionised carbon line [C II] in a luminous quasar host galaxy at $z = 6.6$, 800 million years after the Big Bang. Based on previous studies, this galaxy hosts a $\sim 1 \times 10^9\, M_\odot$ black hole and has a star-formation rate of $\sim 1500\, M_\odot\, \mathrm{yr}^{-1}$. The unprecedented high resolution of the observations reveals a complex morphology of gas within 3 kpc of the accreting central black hole. The gas has a high velocity dispersion with little ordered motion along the line-of-sight, as would be expected from gas accretion that has yet to settle in a disk. In addition, we find the presence of [C II] cavities in the gas distribution (with diameters of ~ 0.5 kpc), offset from the central black hole. This unique distribution and kinematics cannot be explained by a simple model. Plausible scenarios are that the gas is located in a truncated or warped disk, or the holes are created by interactions with nearby galaxies or due to energy injection into the gas. In the latter case, the energy required to form the cavities must originate from the

Очень-очень далекий квазар и его хозяйская галактика

SFR 1500 solar mass per yr

Mazzucchelli et al. 2017). Previous ALMA observations at 0.62″ (3.4 kpc at $z = 6.6$) resolution of the [C II] 158μm emission line and the underlying dust continuum (Venemans et al. 2016) revealed that the black hole is hosted by an ultra-luminous infrared host galaxy (far-infrared luminosity $L_{\rm FIR}$ exceeding $10^{12}\,L_{\odot}$). Based on the dust continuum and the detection of CO(6–5) and CO(7–6) (Venemans et al. 2017), the estimated molecular gas mass in J0305–3150 is $(2.4 - 18) \times 10^{10}\,M_{\odot}$. This gas mass is >60% of the dynamical mass derived from the extent and width of the [C II] line (Venemans et al. 2016), which has a full width at half maximum (FWHM) of 255 km s^{-1}. These earlier observations indicated that the [C II] emission line spectrum shows non-virial motion, consistent with the presence of an outflow or companion galaxy.

Here we present high spatial resolution (0.″076) ALMA observations of the host galaxy of quasar J0305–3150. The pa-

Карта и кинематика в [CII]

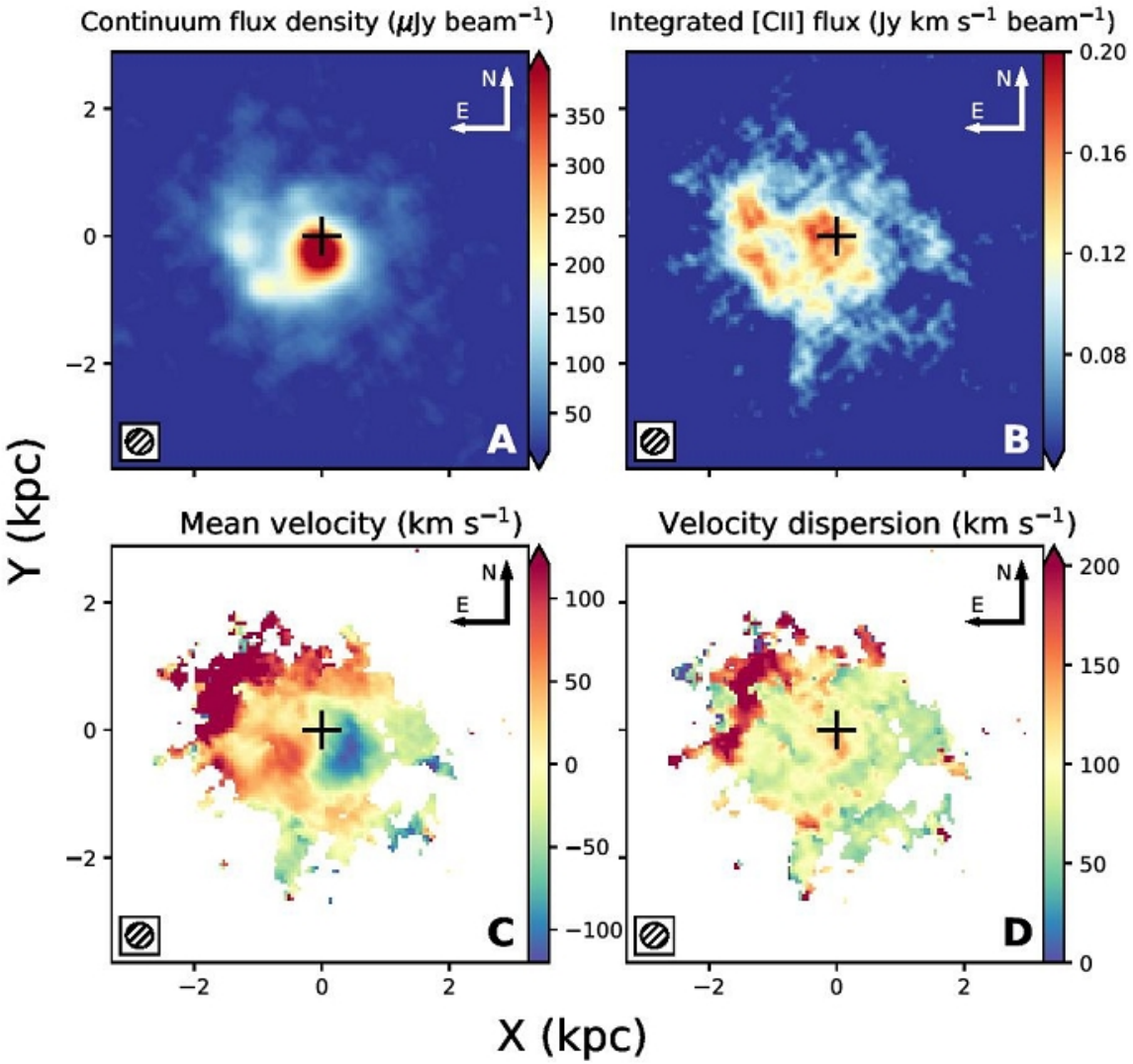

Попытка вписать диск (модели A,B,C и плюс-джет) в поле скоростей

Срезы куба в фиксированных скоростях

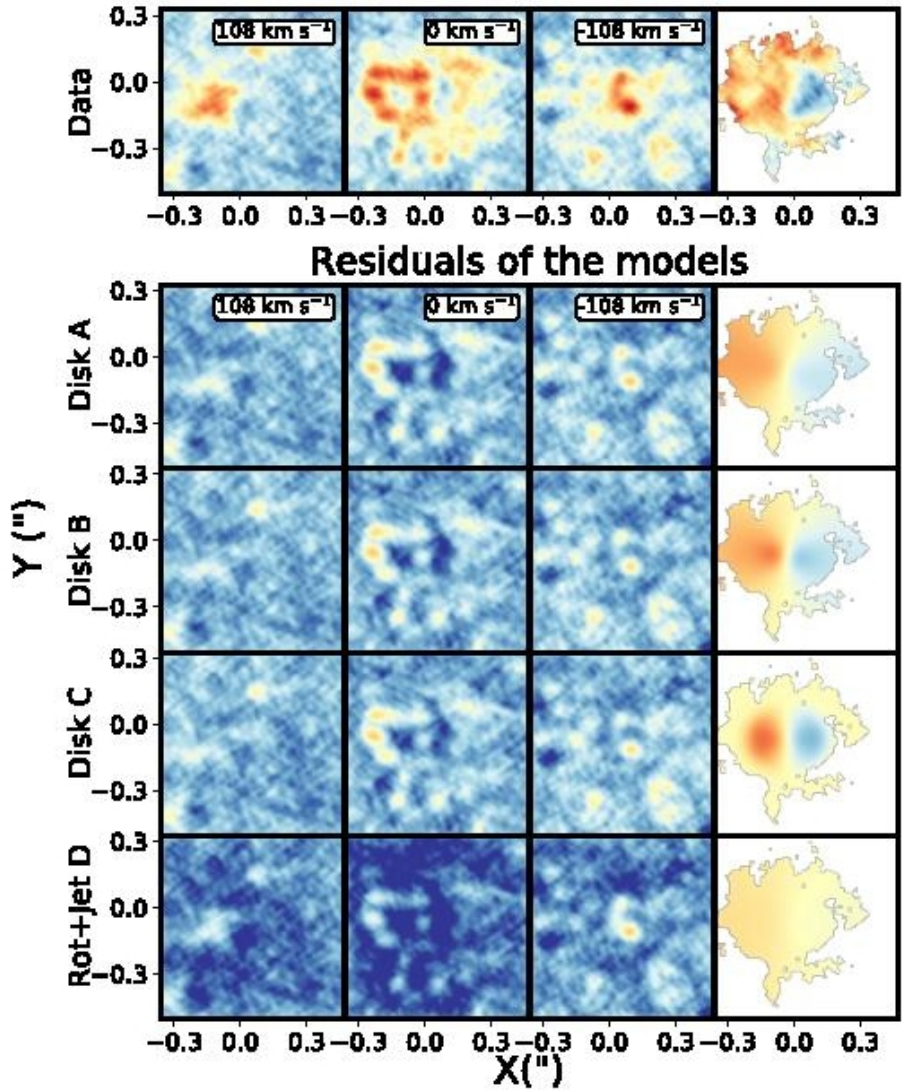

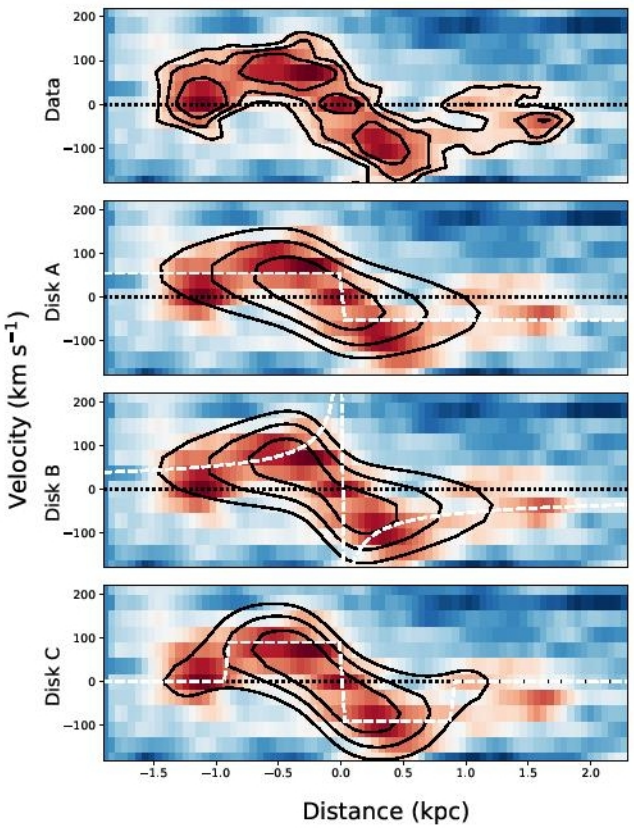

PV-диаграммы вдоль большой оси

По-любому: вся динамическая масса – в газе, и диск должен изгибаться

As can be seen in Figure 3, from the position of the black hole, the velocities increase to a radius of 0.5 kpc (0.1″) and reaches a peak line-of-sight velocity of 150–200 km s^{-1}. Assuming these kinematics can be described by a rotating disk, the dynamical mass within this radius is $M_{\rm dyn} = 2.3 \times 10^9 / \sin^2(i)\,{\rm M}_\odot$, with i the inclination angle of the disk. For comparison, the mass of the black hole is $1 \times 10^9\,{\rm M}_\odot$, and the inferred gas mass within this radius is $1.6 \times 10^{10}\,{\rm M}_\odot$. For an inclination angle of $i = 35°$ (see Table 1), the dynamical mass and molecular gas mass within the central 1 kpc are consistent with each other within the large uncertainties. Beyond this radius, the line-of-sight velocity is decreasing faster than Keplerian (shown by the "Disk B" model in Figure 3), and reaches approximately systemic velocity at the last measured points at 1.5–2.0 kpc. To summarise, the kinematics appear to be dispersion dominated with some overall rotation (i.e. net angular momentum) in the central kpc. This implies that most of the gas has not yet settled in a disk.

Параметры галактики И ЕЕ СОСЕДЕЙ

Table 2. Measured and Derived Properties of the quasar and the Companion Galaxies. All the quoted errors are 1σ and the upper limits are 3σ.

Source:	Quasar	C1	C2	C3	LAE
Right ascension	$03^h05^m16.919^s$	$03^h05^m16.945^s$	$03^h05^m16.868^s$	$03^h05^m16.381^s$	$03^h05^m16.803^s$
Declination	$-31°50'55.901''$	$-31°50'55.728''$	$-31°50'55.220''$	$-31°50'54.980''$	$-31°50'57.300''$
Redshift[a]	6.61391±0.00015	6.6231±0.0003	6.6104±0.0004	6.6066±0.0006	6.629±0.001
Distance (kpc)	—	2.0	5.1	37.4	11.0
Δv_{los}[b] (km s^{-1})	—	+361	−137	−289	+595
$F_{[CII]}$[a] (Jy km s^{-1})	5.43±0.33	0.43±0.05	0.31±0.08	1.13±0.17	<0.23
FWHM$_{[CII]}$ (km s^{-1})	225±15	180±25	135±40	330±55	–
$S_{cont,158\,\mu m}$[c] (mJy)	5.34±0.19	—[d]	<0.23	0.58±0.12	<0.33
$L_{[CII]}$ ($L_\odot$)	$(5.9 \pm 0.4) \times 10^9$	$(4.7 \pm 0.5) \times 10^8$	$(3.4 \pm 0.8) \times 10^8$	$(1.2 \pm 0.2) \times 10^9$	$< 2.5 \times 10^8$
L_{FIR} ($L_\odot$)	$(1.60 \pm 0.06) \times 10^{13}$	—	$<5.2 \times 10^{11}$	$(1.3 \pm 0.3) \times 10^{12}$	$<7.7 \times 10^{11}$
SFR$_{[CII]}$[e] ($M_\odot$ yr^{-1})	1016±73	51±9	35±10	159±28	<25
M_{H_2}[f] ($M_\odot$)	$(1.8 \pm 0.1) \times 10^{11}$	$(1.5 \pm 0.2) \times 10^{10}$	$(1.1 \pm 0.2) \times 10^{10}$	$(3.7 \pm 0.6) \times 10^{10}$	$<7.8 \times 10^9$

[a]The redshift and [C II] line flux ($F_{[CII]}$) are measured using a Gaussian fit to the [C II] line for the quasar and the companions C1, C2 and C3 (as shown in Figure 6). The redshift of the Lyman alpha emitter (LAE) is taken from Farina et al. (2017).

ArXiv: 1903.09591

Cluster induced quenching of galaxies in the massive cluster XMMXCS J2215.9-1738 at $z \sim 1.5$ traced by enhanced metallicities inside half R_{200}

C. Maier[1], M. Hayashi[2], B. L. Ziegler[1], and T. Kodama[3]

[1] University of Vienna, Department of Astrophysics, Tuerkenschanzstrasse 17, 1180 Vienna, Austria
e-mail: christian.maier@univie.ac.at
[2] National Astronomical Observatory of Japan, Osawa, Mitaka, Tokyo 181-8588, Japan
[3] Astronomical Institute, Tohoku University, Aramaki, Aoba-ku, Sendai 980-8578, Japan

Received ; accepted

ABSTRACT

Aims. Cluster environments at $z < 0.5$ were found to increase the gas metallicities of galaxies which enter inner regions of the clusters where the density of the intracluster medium is high enough to remove their hot halo gas by ram-pressure stripping effects and to stop the inflow of pristine gas. To extend these studies to $z > 1$, the most massive clusters known at these redshifts are the sites where these environmental effects should be more pronounced and more easily observed with present day telescopes.
Methods. We explore the massive cluster XMMXCS J2215.9-1738 at $z \sim 1.5$ with KMOS spectroscopy of Hα and [N II] λ6584 covering a region that corresponds to about one virial radius. Using published spectroscopic redshifts of 108 galaxies in and around the cluster we computed the location of galaxies in the projected velocity vs. position phase-space to separate our cluster sample into a virialized region of objects accreted longer ago (roughly inside half R_{200}) and a region of infalling galaxies. We measured oxygen abundances for ten cluster galaxies with detected [N II] λ6584 lines in the individual galaxy spectra and compared the mass-metallicity relation of the galaxies inside half R_{200} with the infalling galaxies and a field sample at similar redshifts.

Объект и его наблюдения на VLT

2.1. KMOS observations and data reduction of cluster SF galaxies in XMM2215

XMM2215 was discovered in the XMM Cluster Survey (Stanford et al. 2006). It is a massive $z \sim 1.46$ cluster with an older estimation of the mass of $M_{200} \sim 2.1 \cdot 10^{14} M_{\odot}$ (Hilton et al. 2010; Stott et al. 2010), and a newer estimation in this study of a higher mass of $M_{200} \sim 6.3 \cdot 10^{14} M_{\odot}$ (see Sect. 3.1). One advantage for observational environmental studies in this cluster compared to other clusters at $z > 1$ is its wealth of spectroscopic redshifts published not only for star forming but also for passive galaxies (Hilton et al. 2009, 2010; Hayashi et al. 2011; Beifiori et al. 2017; Chan et al. 2018). This enables to characterize the accretion state of cluster member galaxies by identifying virialized and infalling regions (see Sect. 3.1).

The targets for the KMOS H-band observations were selected from the list of $1.44 < z < 1.48$ [OII] emitters, with a flux larger than 2×10^{-17}ergs/s/cm^2, identified from narrow-bands NB912 and/or NB921 by Hayashi et al. (2014). Most of the targets have been already spectroscopically confirmed before the KMOS observations. VLT/KMOS H-band observations were carried out in 2016 in the night October 19th/20th with a

Удалось получить эмиссионные спектры для 6 галактик в вириализованной зоне и 5ти – вне ее

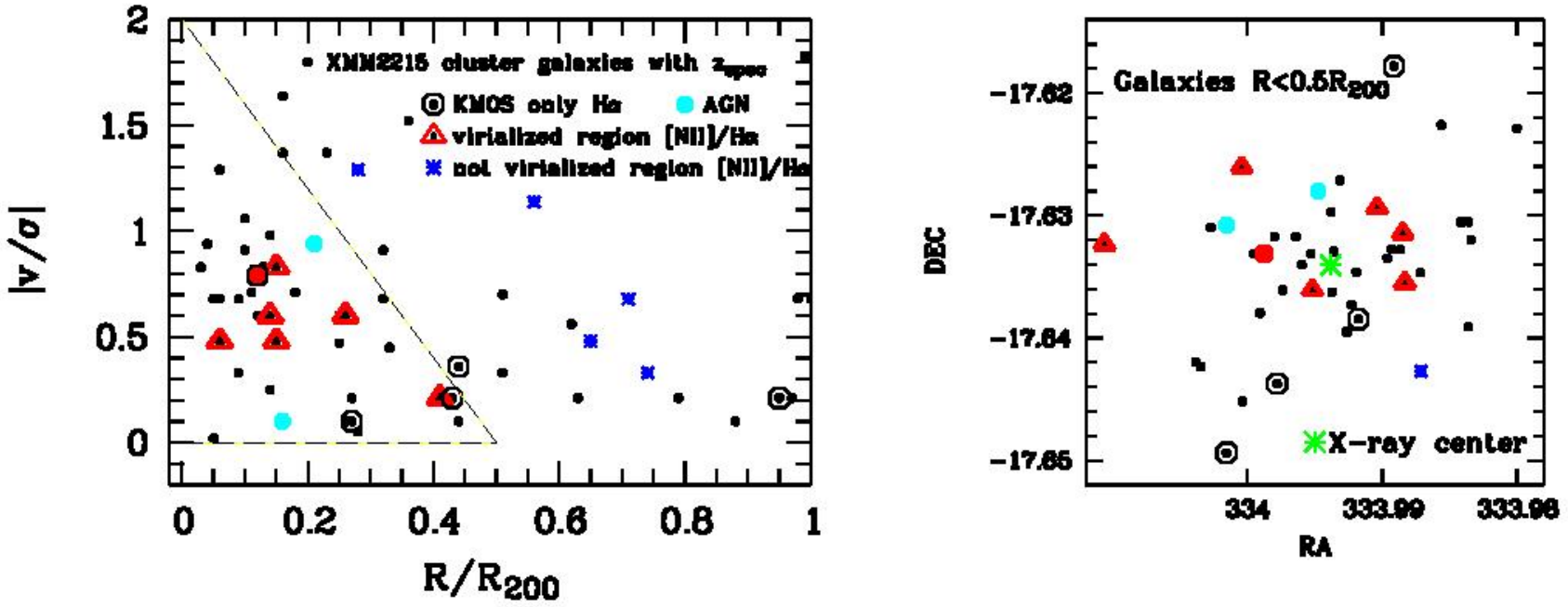

Fig. 2. Left: Phase-space diagram showing 58 XMM2215 cluster galaxies with spectroscopic redshifts inside R_{200}. The galaxies with KMOS H-band observations are shown by larger symbols, as indicated in the legend. The dashed large triangle in the lower left-hand corner shows the virialized region, as derived by Rhee et al. (2017) using cosmological hydrodynamic simulations of groups and clusters. Right: Spatial distribution of 42 galaxies in the central part of the XMM2215 cluster at $R < 0.5R_{200}$ (symbols like in the left panel). The red filled circle indicates one galaxy with measured [NII]/Hα with much higher mass than the galaxies shown as red triangles. A green star symbol shows the cluster center determined with extended X-ray emission (Stanford et al. 2006).

Вроде, у галактик в центре скопления – повышенная металличность газа

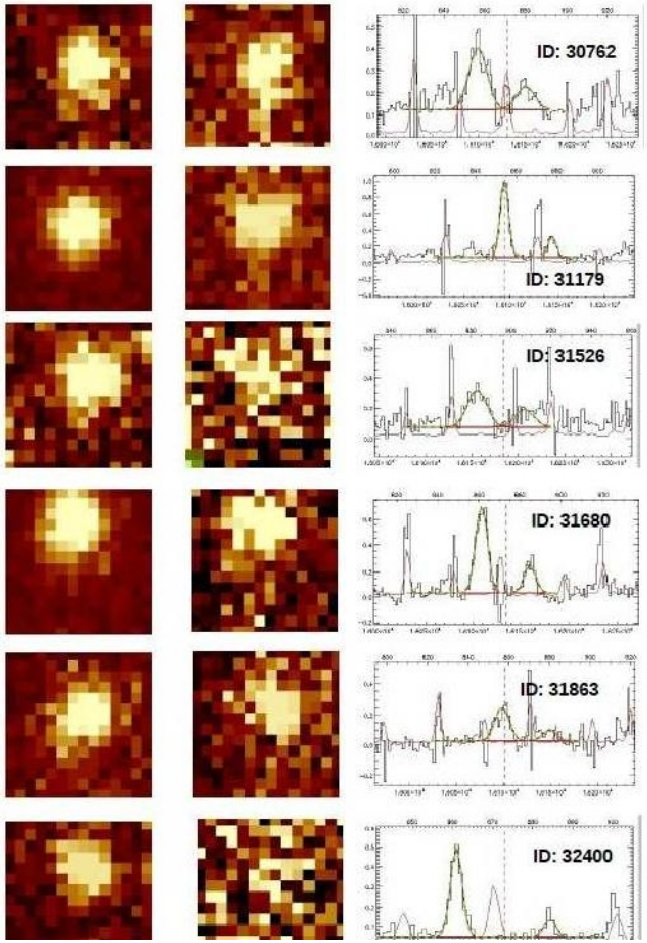

H-alpha [NII]

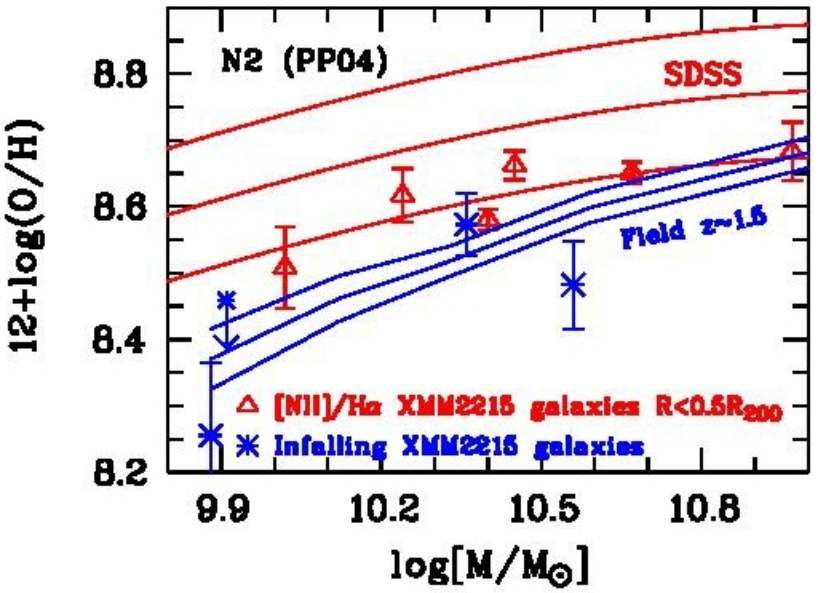

Fig. 4. MZR for cluster and field galaxies at $z \sim 1.5$, using the N2-method of Pettini & Pagel (2004) to derive oxygen abundances. The SDSS local MZR relation is shown by the red solid lines using the fit given by Kewley & Ellison (2008) for the N2 calibration. The blue solid lines show the mean location of field galaxies at $z \sim 1.5$ from Kashino et al. (2017). Red triangles are XMM2215 cluster galaxies from the *SFvirialized* sample, while blue star symbols are XMM2215 infalling galaxies (see phase-space diagram, Fig. 2).

ArXiv: 1903.10514

NGC 1380

The Fornax 3D project: a two-dimensional view of the stellar initial mass function in the massive lenticular galaxy FCC 167

I. Martín-Navarro[1,2], M. Lyubenova[3], G. van de Ven[3,4], J. Falcón-Barroso[5,6], L. Coccato[3], E. M. Corsini[7,8], D. A. Gadotti[3], E. Iodice[9], F. La Barbera[9], R. M. McDermid[10,11], F. Pinna[5,6], M. Sarzi[12,13], S. Viaene[13,14], P. T. de Zeeuw[15,16], and L. Zhu[2]

[1] University of California Observatories, 1156 High Street, Santa Cruz, CA 95064, USA
e-mail: imartinn@ucsc.edu
[2] Max-Planck Institut für Astronomie, Konigstuhl 17, D-69117 Heidelberg, Germany
[3] European Southern Observatory, Karl-Schwarzschild-Str. 2, 85748 Garching b. München, Germany
[4] University of Vienna, Department of Astrophysics, Türkenschanzstrasse 17, 1180 Vienna, Austria
[5] Instituto de Astrofísica de Canarias,c/ Vía Láctea s/n, E38205 - La Laguna, Tenerife, Spain
[6] Departamento de Astrofísica, Universidad de La Laguna, E-38205 La Laguna, Tenerife, Spain
[7] Dipartimento di Fisica e Astronomia 'G. Galilei', Università di Padova, vicolo dell'Osservatorio 3, I-35122 Padova, Italy
[8] INAF–Osservatorio Astronomico di Padova, vicolo dell'Osservatorio 5, I-35122 Padova, Italy
[9] INAF–Osservatorio Astronomico di Capodimonte, via Moiariello 16, I-80131 Napoli, Italy
[10] Department of Physics and Astronomy, Macquarie University, Sydney, NSW 2109, Australia
[11] Australian Astronomical Observatory, PO Box 915, Sydney, NSW 1670, Australia
[12] Armagh Observatory and Planetarium, College Hill, Armagh, BT61 9DG, UK
[13] Centre for Astrophysics Research, University of Hertfordshire, College Lane, Hatfield AL10 9AB, UK
[14] Sterrenkundig Observatorium, Universiteit Gent, Krijgslaan 281, B-9000 Gent, Belgium
[15] Sterrewacht Leiden, Leiden University, Postbus 9513, 2300 RA Leiden, The Netherlands
[16] Max-Planck-Institut fuer extraterrestrische Physik, Giessenbachstrasse, 85741 Garching bei Muenchen, Germany

MUSE: S/N=100: Новый метод спектрального фиттинга линий

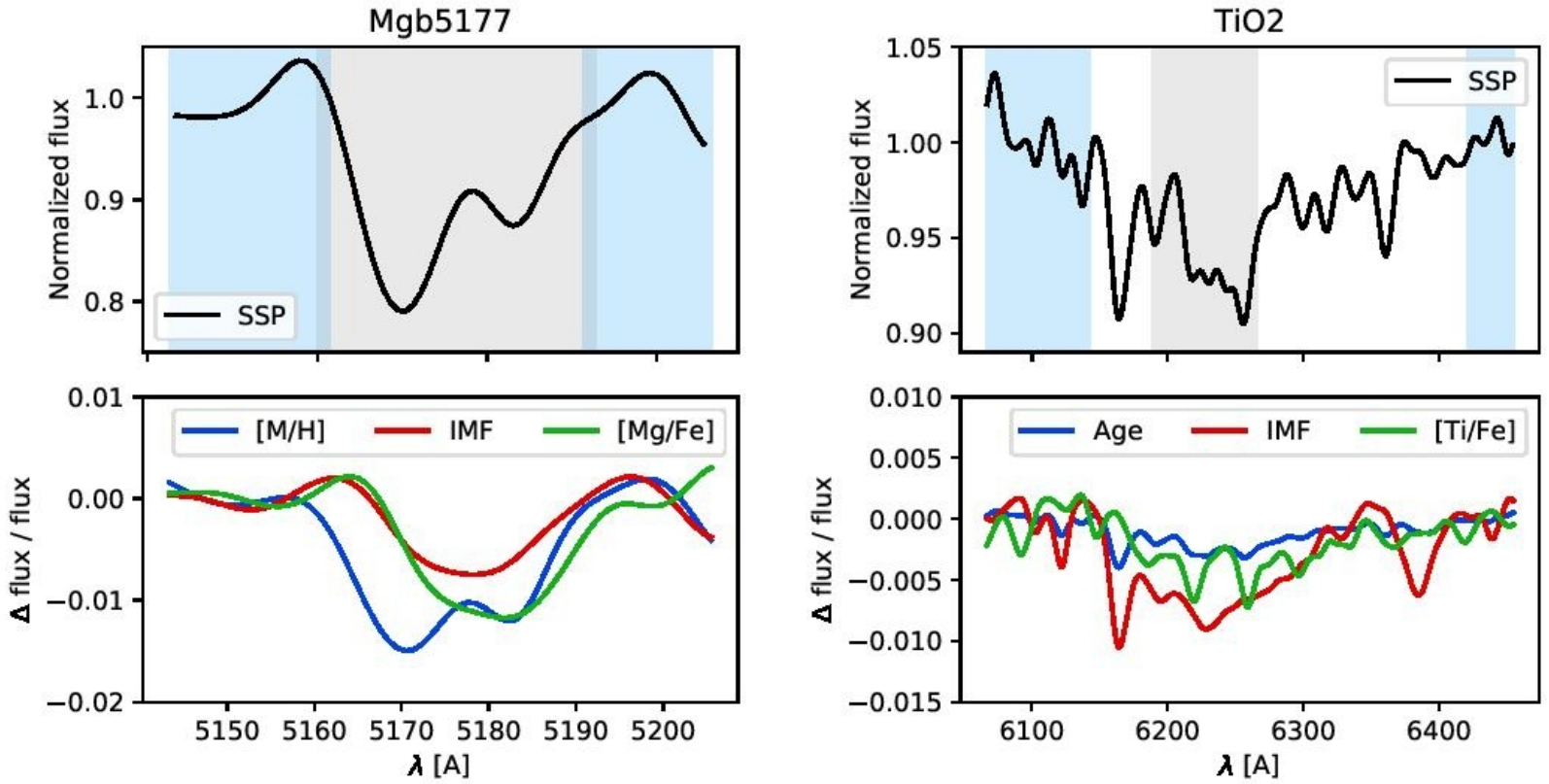

Fig. 1. The full-index-fitting (FIF) approach. The top panels show the Mgb 5177 (left) and the TiO_2 (right) spectral features, normalized using the index pseudo-continua (blue shaded regions). In the FIF approach, every pixel within the central bandpass (grey area) is fitted to measure the stellar population parameters. The black line correspond to a model of solar metallicity [M/H]=0, [Mg/Fe]=0, [Ti/Fe]=0, and Kroupa-like IMF, at

4 свободных параметра, и вырождения не видно

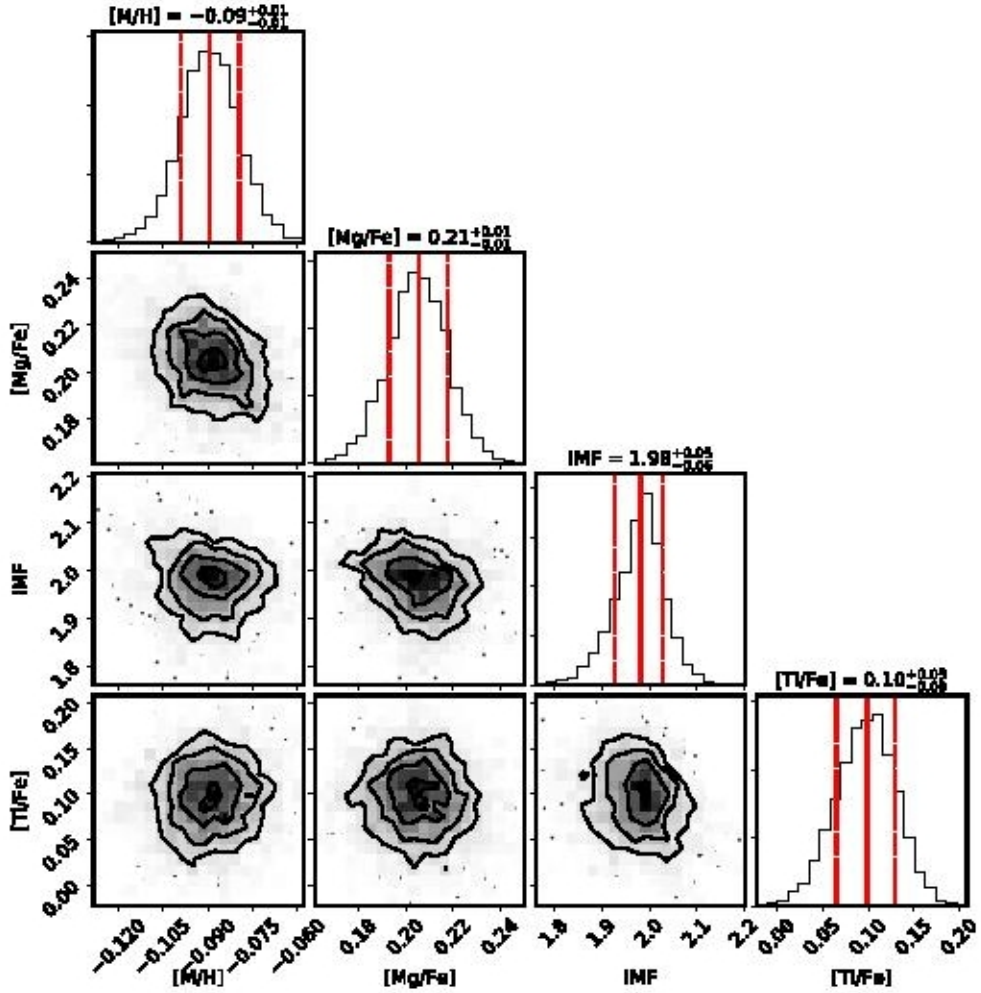

Карты параметров звездного населения – от ядра (слева) до границы диска (справа)

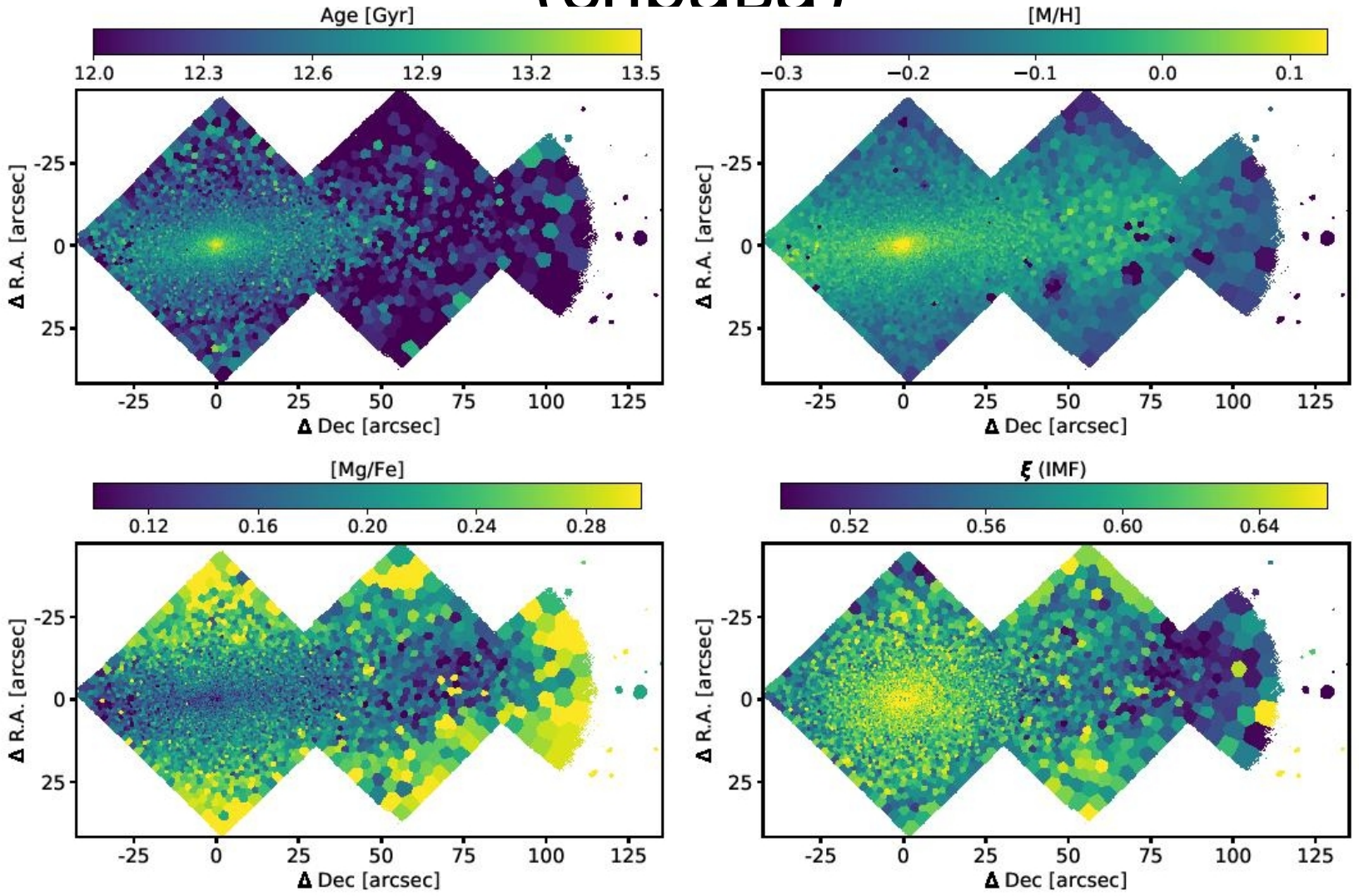

Fig. 4. Stellar population maps of FCC 167. The top left panel shows the age map, as measured from pPXF, where the presence of a relatively old

Основная забота – что движет IMF?

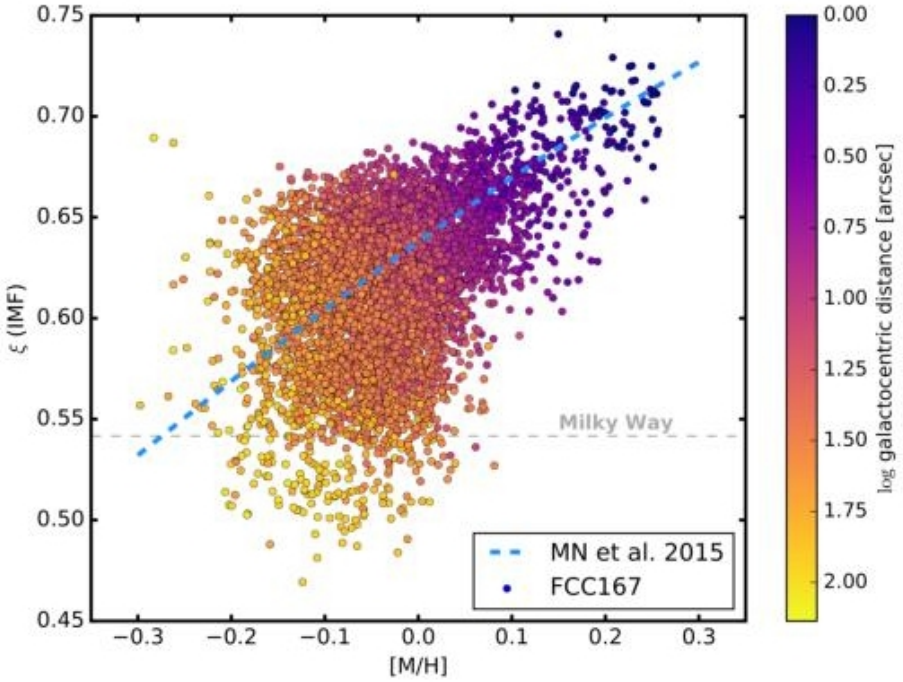

Fig. 5. IMF – metallicity relation. The individual bins of FCC 167 are shown color-coded by their distance to the center of the galaxy, compared with the empirical relation of Martín-Navarro et al. (2015d), shown as an blue dashed line. This relation agrees with the FCC 167 measurements in the central regions of the galaxy (top right corner), but it does not hold for the outskirts, where an additional parameter is needed to explain the observed variations in the IMF. The ξ ratio of the Milky Way (Kroupa 2001) is shown as a grey dashed line.

Не (только) металличность!

Разная форма изолиний параметров

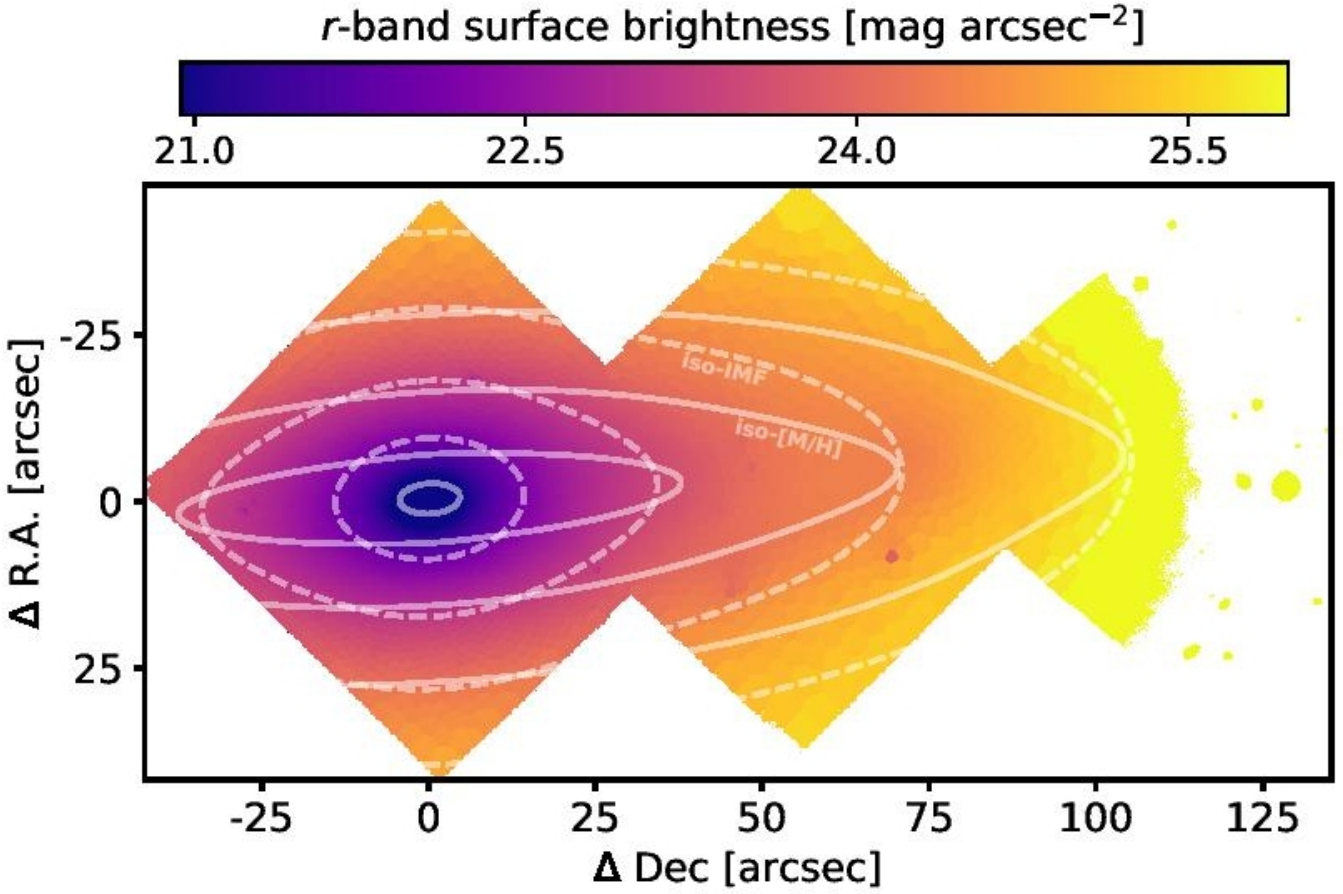

Fig. 6. Iso-metallicity vs iso-IMF contours. The surface brightness map of FCC 167 is shown, as measured from the F3D data cube, with the iso-metallicity (solid lines) and iso-IMF contours (dashed lines) over-plotted. As in Fig. 4, this figure shows how the two-dimensional IMF map

Сопоставление со структурой: химия связана с тонким звездным диском, а IMF - с толстым звездным диском